2022

Atmospheric Air Plasma Streamers Deliver Nanosecond Pulses for Focused Electroporation

Shu Xiao
Old Dominion University, sxiao@odu.edu

Carol Zhou
Old Dominion University, czhou@odu.edu

Eric Appia
Old Dominion University, kappi002@odu.edu

Shirshak Dhali
Old Dominion University, sdhali@odu.edu

Original Publication Citation

Xiao, S., Zhou, C., Appia, E., & Dhali, S. (2022). Atmospheric air plasma streamers deliver nanosecond pulses for focused electroporation. *Bioelectricity*, *4*(4), 198-206. https://doi.org/10.1089/bioe.2022.0025

BIOELECTRICITY
Volume 4, Number 4, 2022

DOI: 10.1089/bioe.2022.0025

Open camera or QR reader and scan code to access this article and other resources online.

Atmospheric Air Plasma Streamers Deliver Nanosecond Pulses for Focused Electroporation

Shu Xiao, PhD,[1,2] Carol Zhou, BS,[1] Eric Appia, ME,[2] and Shirshak Dhali, PhD[2]

Abstract

Background: For electrotherapies that involve electrodes and high-intensity electric fields, such as in tissue ablation, we report a method of pulse delivery that can focus the electric field away from the electrodes, as demonstrated *in vitro*.

Materials and Methods: To electroporate cells in a monolayer seeded in a 35 mm culture dish, two atmospheric-pressure plasma channels generated by two thin, copper foil electrodes above the surface of the solution provided the current and established the electric field.

Results: Depending on the pulse duration, the plasma channels were observed as corona (100 ns), streamer (300 ns), and mixture of streamer and arc (1 μs). With the Yo-pro-1 and propidium iodine uptakes as electroporation markers, the corona plasma did not cause observable electroporation. The streamer and arc mixed plasma allowed a large area of monolayer cells to be electroporated. Only the streamer channels allowed the focused electroporation of the cells at the center area on the culture dish, while the areas directly under the electrodes showed weak or no response. It is a desired effect that could not be achieved by electrodes directly touching cells or cell solution.

Conclusion: The focused poration was most likely caused by nanosecond pulsed electric fields, not by plasma chemistry.

Keywords: streamer, discharge, nanosecond pulses, electroporation

Introduction

The electromanipulation of macromolecules, cells, and organisms has gained large momentum in recent bioengineering research and applications. Central to any electromanipulation is the establishment of an electric field. When high-curvature electrodes deliver high-voltage pulses to a tissue, which is the case for electroporation requiring an electric field from 0.1 to 100 kV/cm,[1] the field near the electrodes is much higher than that in the bulk region. Targeting a lesion in the electrode gap while sparing the tissues near the electrodes will not be achieved. For example, a treatment on the skin often leaves an electrode mark and could cause a long-lasting cosmetic issue. Furthermore, unwanted effects such as charge emission, pressure wave emission, and joule heating and bubble generation may occur.[2,3]

In tissue ablation, an electrode array can increase the inter-gap electric field and mitigate the inhomogeneity problem.[4,5] An optimized eight-electrode array produced a larger ablation zone than a single electrode when the same electrical pulse was delivered.[6] In the application of nonpenetrating skin electrodes for DNA vaccination, a multielectrode array (MEA) was developed,[7] which divided the target area into several smaller segments for better efficiency and homogeneity. Also, for the purpose of gene electrotransfering to the skin, a noninvasive MEA was developed.[8] An electrode array is effective in increasing

[1]Frank Reidy Research Center for Bioelectrics and [2]Department of Electrical and Computer Engineering, Old Dominion University, Norfolk, Virginia, USA.

the electric field between the electrodes, but the local electric field adjacent to the electrodes is still significantly higher.

Therefore, the electrode array does not eliminate the field enhancement problem. Recently, a new modality named cancellation of cancellation (CANCAN) was shown to suppress cell responses near the electrodes by bipolar pulses while retaining the remote responses with unipolar pulses.[9,10] This modality is based on the nanosecond bipolar cancellation phenomenon, in which a cell response caused by unipolar nanosecond pulses is suppressed by subsequent pulses with reversed polarity.[11–16] The CANCAN regimen can be useful for various electrical conditions and endpoints, but the problem of electric field enhancement near the electrodes persists and the cell response caused by the first phase is too strong to be cancelled by the following reversed phase.

One way to solve the problem is to avoid the direct contact of the electrodes with the targeted tissue and utilize the leakage field. For example, by lifting a pair of needle electrodes above a piece of skin, the leakage field below the needle electrodes no longer reflects the electrode geometry, and in fact appears to be focused in an oval shape with the greatest magnitude at the center.[17] Accordingly, the ''footprints'' of the needles projected to the skin would change into that oval shape overlapping the lesion to be treated, therefore allowing the electrode mark to be removed. However, since the air is an insulator, the leakage field in the skin would be too small. An improved scenario would be having a conductive medium between the elevated needles and the skin. This idea inspired us to use a pair of electrodes through a ''self-generated'' air plasma (ionized gas) to deliver high-intensity fields.

The electrodes, energized by high voltage pulses, emit plasma for conductance and provide the required electric pulses. Depending on the ionization degree and range, the plasma can be in the mode of a corona (low-level ionization, near electrodes), a streamer (medium ionization, bridging the interelectrode gap), or an arc (high ionization, bridging the interelectrode gap), which can be controlled by varying the pulse duration. These plasma types are composed of a number of filamentary discharges, although glow discharges with more spatially uniform discharges may be used, which, however, involve different electrode configuration and pulse condition. In principle, a plasma electrode (PE) has the following advantages over a metal electrode (ME). First, the electric field gradient near the plasma front is arguably smaller than that of an electrode with a high curvature and sharp edges.

Although the electric field associated with the plasma front could be three to four times greater than the average field due to the space charge effect, such field enhancement is short-lived (several nanoseconds)[18] and would not cause a long-lasting effect to the cells. Second, the conduction of the current takes the form of many branches, which tends to thin out the current density and lower the local electric field. Third, the plasma initiates from different sites on the electrode surface from pulse to pulse, which can reduce the chance of forming a persistent single hot spot found in the ME. Finally, the local change in the concentration of the ions can be avoided without the interaction between a metal and the solution. These features are conducive to a remote and targeted treatment of a lesion and will thus reduce or avoid the unwanted collateral damages to the nearby healthy tissues.

In an *in vitro* setting, we tested the PE and demonstrated its capability of focusing the electric field for remote electroporation. We used two curved foil electrodes powered by high-voltage nanosecond pulses to generate atmospheric pressure air plasma channels and to deliver the same pulses to the monolayer cells seeded in a culture dish. The plasma channels touched the solution and established the electric field required for the cell membrane poration. A focused electroporation at the culture dish center was shown with the PE, but not with the ME. Interestingly, only the streamer channels created by the 300 ns pulses caused the focused electroporation.

We note that numerous articles have been published on the air plasmas and their applications in biochemistry and medicine. One of the main underlying mechanisms is the plasma chemistry associated with chemically active species (reactive oxygen species and/or reactive nitrogen species, or atoms).[19] But in the context of our approach, the plasma chemistry did not seem to be the primary mechanism. Rather, the electric field delivered by the PE was responsible for the observed focal electroporation.

Materials and Methods

Electric pulses (100 ns–1 μs) were delivered by the PE or the ME to the monolayer cells (Chinese Hamster Ovarian, CHO cells) seeded on the 35 mm culture dishes. The electric parameters, including voltages, currents, and electric fields, were measured with high-speed sensors and an oscilloscope. The electroporation of cell membranes was measured by the uptakes of Yo-pro-1 and propidium iodide (PI). The possible generation of reactive species was evaluated by the degradation of indigo carmine (IC) after the PE treatment through the ultraviolet-visible absorption spectra.

Electrode configurations

The PEs were made of two square copper foil electrodes with a width of 1.4 cm and a thickness of 66 μm adhering to the outer surface of a polyvinyl chloride (PVC) cylinder with the outer diameter of 2.15 cm and the inner diameter of 1.5 cm (Fig. 1a, b). They faced each other with a separation of 180° in the azimuthal direction. The bottom edges of the copper foils were 3 mm from the end of the PVC cylinder. In the experiments, the end of the PVC cylinder was brought to touch the surface of the solution inside the culture dish by a micromanipulator, while keeping the dish and the cylinder concentric. The plasma channels emitted from the electrodes made the contact with the cell solution when the copper foils remained in air. To compare the spatial distribution of electroporation with that caused by the ME, a pair of square metal (aluminum) electrodes with a gap distance of 1.94 cm, which is approximately the same as the PE foil distance (Fig. 1c), were used for separate electroporation experiments. In that case, the ME only touched the solution surface and was not immersed in it.

Pulse generator and electrical measurements

The electric pulses to energize the PE ranged from 100 ns to 1 μs. The pulses were generated by a patented technology,[20,21] which is a solid-state Marx-bank generator consisting of several MOSFET switch stacks. These stacks are turned on simultaneously to discharge a series of pre-charged capacitors

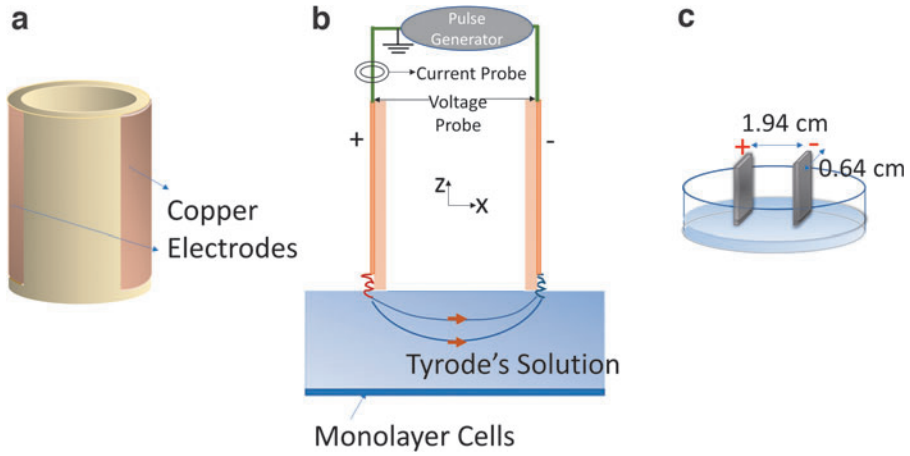

FIG. 1. The electrodes used for the experiments. **(a)** In the PE, a pair of square-shaped copper foil electrodes adhered on the outer surface of a PVC cylinder. **(b)** The electrodes were 3 mm above the solution and connected to a nanosecond pulse generator. **(c)** As a comparison, a pair of square-shaped aluminum electrodes (ME) were used to electroporate the monolayer cells. The electrodes only touched the surface of Tyrode's solution. ME, metal electrode; PE, plasma electrode; PVC, polyvinyl chloride.

(5 kV) and to boost the combined voltage to 15 kV (maximum). The polarity of the output high voltage is negative with respect to the earth potential. The high-voltage side was applied to one of the foil electrodes (the cathode), and the ground lead was connected to the opposing foil electrode (the anode). The pulses were delivered at 2 Hz for three treatment times: 30 s, 1 min, and 2 min.

The electric currents were measured with a wideband current sensor (Model 411; Pearson), and the voltages were measured with a high-voltage probe (P6015A; Tektronix). The electric field was measured with a fiber-optic probe based on the Pockels effect (eoSense, HF-10V-2-AMP; Kapteos, France), where the change in the refractive index of the fiber tip due to field stress was recorded and then converted proportionally to the applied electric field. To accommodate the probe and the attached optic fiber, a plastic container was used instead of the 35 mm culture dish. The saline with the same conductivity as Tyrode's solution was added to the container.

The sensitive region of the probe, according to the manufacture datasheet, is a cylinder of 4 mm in diameter and 1.75 cm in length. Using a parallel electrode gap, we calibrated the probe and identified the linear range to be less than 1.5 kV/cm. Higher electric fields caused the probe to saturate with an artifact tail after the signal. To measure the *x*-component of the field, the probe was oriented in the *y* direction under the PVC cylinder while being moved in the *x* direction.

Cell culture and membrane integrity test

The electroporation resulting from the PE or the ME was assessed on CHO cells. This cell line has been extensively studied with nanosecond electric pulses and proved to be stable and robust.[22] Cells with passage numbers between 12 and 30 were propagated on average over ~72 h at 37°C with 5% CO_2 in air and the Kaighn's Modification of Ham's F-12 Medium (302004; ATCC, Manassas, VA) supplemented with 10% fetal bovine serum, 2-mM L-glutamine, and 100-U/mL penicillin/streptomycin. For 20 h, the cells grew into a single layer covering the entire area of the culture dish. In the experiment, Tyrode's solution was used. A volume of 1.5 or 3 mL was used to control the cell depth to be 1.5 or 3 mm.

The poration of cell membranes was measured with the uptake of the fluorescent markers Yo-pro-1 dye and PI in separate experiments. They were added to the cell solution before the experiment. After pulsing, the solution was kept for 10 min before the cells were washed and taken for the fluorescence microscopy.

In the first series of experiments, the Yo-pro-1 uptake was obtained with an inverted fluorescence microscope (IX71; Olympus) with a magnification ratio of 4×. A total of 13 points were scanned on the *x* and *y* axes for the spatial distribution of the uptake, and each point represented an area of 2.2 × 1.6 mm. In the later experiments, the Yo-pro-1 uptake data and the PI data were gathered with a widefield, motorized fluorescence microscope (Dmi8; Leica) with a magnification ratio of 5×.

Plasma chemistry

IC powder was dissolved in Tyrode's solution. It was added to the culture dish for the PE treatment for various times (from 30 s to 10 min). No cells were placed in the culture dish. The treated solution was afterward allocated in the 36-well plates to measure the absorption spectra with a plate reader (285–1000 nm, SpectraMax i3; Molecular Devices).

Data analysis and statistics

After the fluorescence images were obtained, the quantitative analyses of Yo-pro-1 and PI uptakes were conducted with the ImageJ (Version 1.53e). For images taken at the discrete points, the fluorescence was averaged over the captured area. For the widefield images, the line scanning on the *x*-axis and *y*-axis resulted in a two-dimensional distribution of the uptakes. All the quantitative data include the mean values and standard error bars.

Results

Plasma generation by the PE

The plasma channels produced from the anode and the cathode formed in three modes: a corona, a streamer, and an arc, depending on the pulse duration, whereas the pulse amplitude (peak: 12 kV) was kept the same (Fig. 2a, b). For all types of plasma channels, it took ~70 ns for them to form, indicated by the delay of the current rise after the voltage was applied with the same voltage rise (0.125 kV/ns).

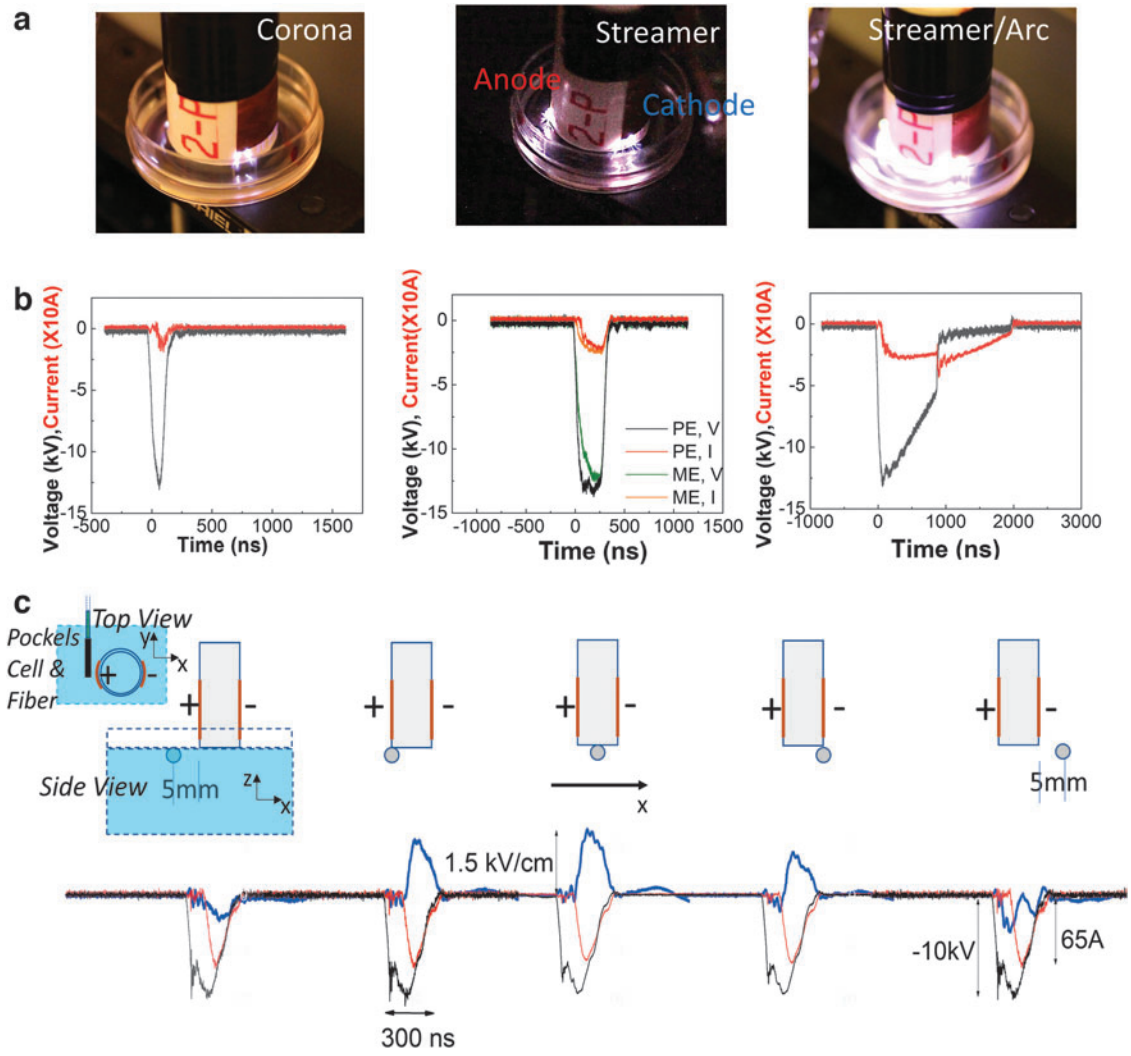

FIG. 2. Plasma channels were produced with the electrodes (Fig. 1a) for the pulse durations of 100 ns, 300 ns, and 1 μs **(a)**. The corresponding currents and voltages are shown in **(b)**. The voltage and current in the ME case were added for comparison with the PE. The electric fields **(c**, blue line) were measured for five positions under the PVC cylinder in the solution for the streamers produced by the 300 ns pulses **(c**, voltage: black line; current: red line). The positions of the fiber-optic field sensor are indicated by the shaded circles. Note that the container for **(a)** was 35 mm culture dishes, different from that for **(c)**, so the voltage and current levels were different.

The corona channels, generated by the 100 ns pulses, appeared to be the weakest in terms of the brightness, as the plasma could barely make it to the surface of the solution. The streamer channels, produced by the 300 ns pulses, were brighter and more energetic. They reached the solution surface and dispersed into multiple smaller streamers. For the 1 μs pulses, the plasma channels were a mixture of streamers and arcs, as indicated from the collapsed voltage (Fig. 2b). For the electrodes shown in Figure 2 and in all three cases (corona, streamer, and arc), the brightest filaments are located at the corners of the electrodes, but many dimmer filaments can stem from the middle sections. For other electrodes, the brightest filaments could appear in the middle sections, not necessarily always at the corners.

Electric fields in the solution

The electric fields (the x-component) in the solution at five locations, the exact center, under the electrodes (both the anode and the cathode), and away from the electrodes (5 mm from the PVC cylinder), are shown in Figure 2c. These results were for the 300 ns pulses. In general, the fields at all locations started out with a delay after the application of the voltages and coincided with the rise in the currents. The field at the center location was the largest and reached 1.5 kV/cm, the saturated value of the probe. The saturation was also indicated by a tail pulse, which is an artifact as both the current and the voltage signals disappeared, so the actual field magnitude could be much higher. At the positions 5 mm from both the anode and the cathode, the fields dropped to 0.5 kV/cm.

Electroporation of cell membranes

The Yo-pro-1 uptakes of monolayer cells (CHO cells) are shown in Figure 3. These results, the fluorescence intensity and distribution, exhibited a dose-dependent manner. For the 100 ns plasma, no uptake was observed no matter how many

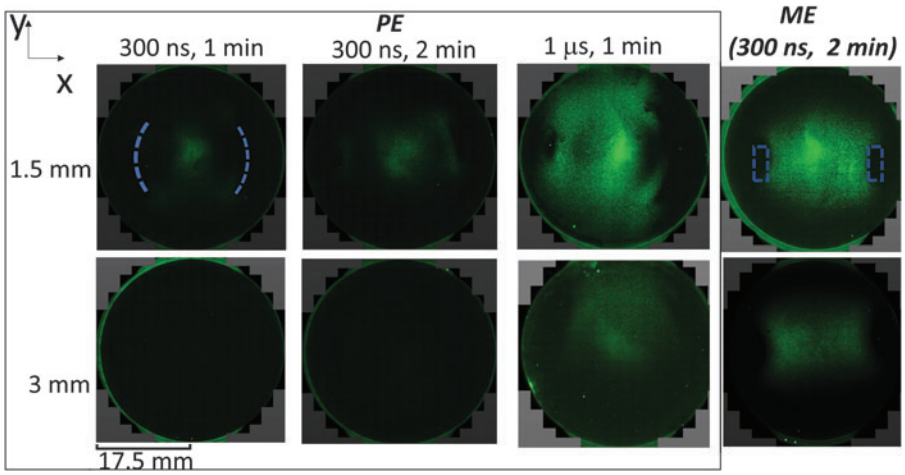

FIG. 3. The Yo-pro-1 uptakes of the monolayer Chinese Hamster Ovarian cells seeded in the 35 mm culture dishes after treatment by the PE. The projected electrode footprints on the dish surface are indicated by the dashed lines. The treatment conditions varied from 300 ns to 1 μs for different exposure times (1–2 min). The cells were at two depths (1.5 mm, top row; 3 mm, bottom row). As a comparison, an electrode pair (ME) was used to treat the cells in separate experiments. The MEs (the position indicated by the dashed lines) were touching the solution, but not immersed in it. The pulse rate was 2 Hz in all cases.

pulses were applied. Hence, the uptake images are not shown. For the 300 ns plasma, the uptake was seen after the 1- or 2-min treatment and was focused at the dish center. This is clearly a remote effect as the electrodes were 3 mm above the solution and away from the dish center. Although there were still some uptakes near the footprints of the electrodes (dashed lines), they are smaller than the center uptake.

By comparison, the uptake caused by the ME, which directly touched the solution (not the cells, as the ME were still 1.5 mm above the dish bottom where cells were seeded), was widespread between the electrodes. The abrupt change from the no-uptake (dark) region to the uptake (green) region clearly reflects the electrode shape. The difference in uptakes can be better seen in the quantitative data (Fig. 4) in which the abrupt increase of Yo-pro-1 uptake is seen on the *x*-axis (Fig. 4b).

For the 1 μs-plasma treatment of 1 min, the uptake was much stronger than that for the 300 ns plasma, although the focal effect disappeared. Also, the uptake did not reflect the electrode footprints as did for the ME (Fig. 3). At the increased cell depth (3 mm), the uptakes by the 300 ns plasma almost vanished, but the 1 μs-plasma still created a visible Yo-pro-1 uptake. To reach a broader and deeper electroporation, the 1 μs-plasma may seem a good option. However, other mechanisms, such as shock waves, may complicate the electroporation pattern. For the ME, the uptake was also obvious compared with that for the 300 ns plasma, suggesting that the ME could reach deeper than the PE for the same applied pulse voltage.

The PI uptake images for the 300 ns plasma are shown in Figure 5. With the same electrical pulse, the uptake increased as the treatment time increased, but not exactly in a linear manner. For example, the peak PI uptake in the *x*-direction was 7 (arbitrary unit) for the 30 s treatment, 22 for 1 min, and 35 for 2 min. The rate of increase was thus almost twice as large in the first minute than that in the second minute.

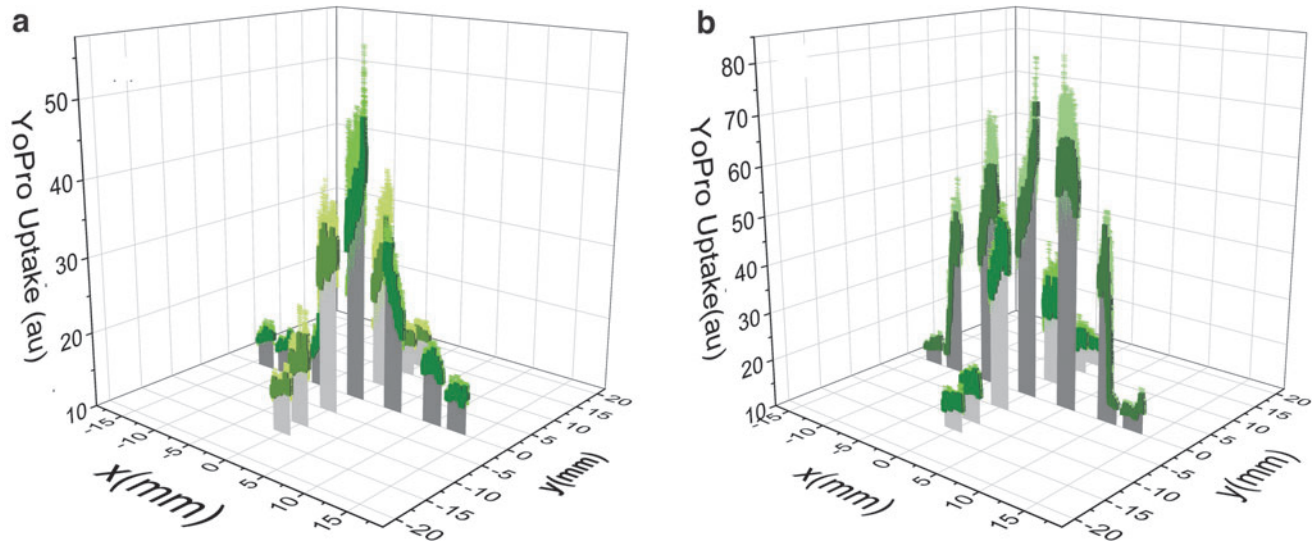

FIG. 4. The quantitative Yo-pro-1 uptake distributions obtained from the cells at 1.5 mm. **(a)** The results ($N=8$) for the 300 ns pulses delivered by the PE after a treatment of 240 pulses (2 min, 2 Hz, see a typical fluorescence image in Fig. 3). **(b)** The results ($N=8$) for the 300 ns pulses delivered by the ME after a treatment of 240 pulses (2 min, 2 Hz, see a typical fluorescence image in Fig. 3).

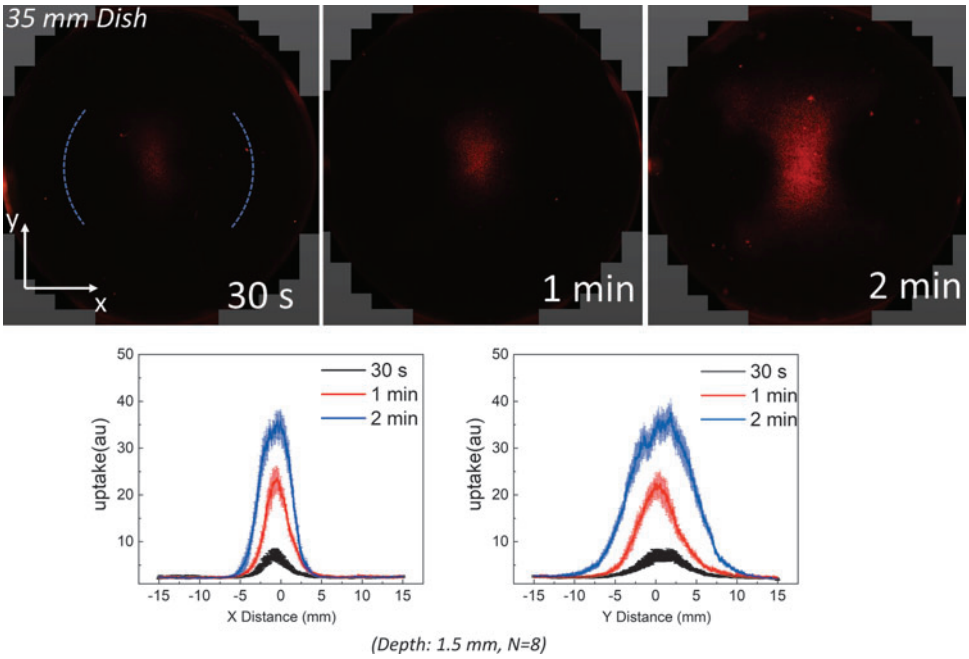

FIG. 5. The images of the propidium iodide uptake (widefield images; Leica) for the 300 ns plasma after the treatment for 30 s, 1 min, and 2 min. The corresponding uptake distributions for the *x* and *y* axes are also shown. The pulse rate was 2 Hz in all cases.

Irrespective of the treatment time, the PI uptake remained focused at the center of the culture dish and was distant from the electrodes, which is consistent with the results of the Yo-pro-1 uptake. Based on the PI uptake data (Fig. 5), the focal spot can be estimated to be a 4×6 mm oval (width of the 50% drop of the uptake). The oval shape has a dependence on the configuration of the foil electrodes, for which streamers were more likely to initiate from the foil corners than the bottom flat edge.

Plasma chemistry test

The reactive species are generally regarded as the primary mechanism in the plasma medicine to kill pathogens or cells. Such a mechanism could also occur in the PE when delivering the pulses to the solution (Fig. 6a–c). To detect the potential existence of reactive species, IC was chosen as a marker to observe the color removal,[23,24] if any, due to the PE treatment. The C = C double bond of the IC molecule can be

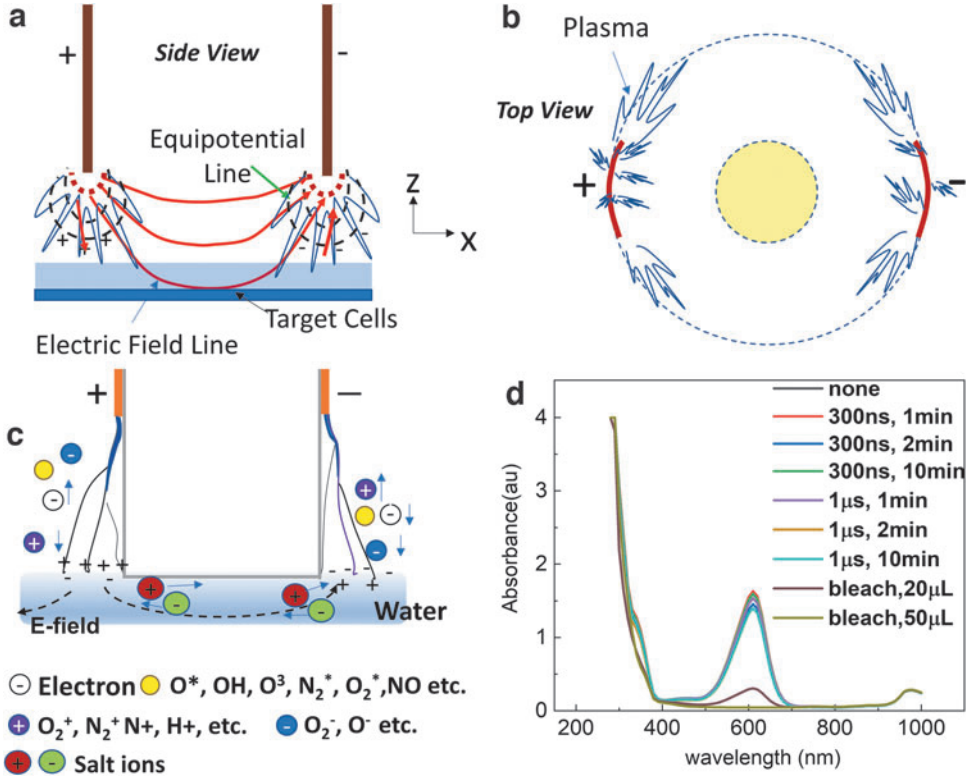

FIG. 6. The physical and chemical conditions for the PE treatment. **(a, b)** The side view and top view of the PE during a treatment. The electric field associated with the plasma is analogous to that generated by a pair of elevated electrodes. **(c)** The electric charges and chemical active species in the interface between the PE and the water. **(d)** Absorbance of lights by an indigo carmine solution after the treatment of the PE for various treatment conditions.

broken by free radicals, such as H_2O_2 or O_3, and therefore loses the red color. Here, in the positive control treated with a detergent, the IC solution showed complete decolorization. However, the PE treatment did not cause a change in the absorbance over the entire spectrum for all pulse conditions (300 ns or 1 μs pulses; Fig. 6d). This was the case even when the treatment lasted for 10 min, far longer than the treatment time (<2 min) in Figures 3 and 5, where the Yo-pro-1 uptake and the PI uptake were measured. This result suggests that the IC molecule was intact, and the role of the plasma-generated free radicals was negligible.

Discussion

This work demonstrated that nanosecond pulses delivered by the PE to monolayer cells generated focused remote response, which in this case, was the poration of cell membranes measured with the Yo-pro-1 and PI uptakes. In contrast, the electroporation caused by the ME did not have such a focal pattern and the electrode profile can be clearly seen. Thus, the PE has the advantages of focused treatment and elimination of electrode footprint, which confirms the postulations laid out in the Introduction section.

Unlike a typical plasma device which interacts with tissue/solution through mechanisms such as reactive species (reactive oxygen species or nitrogen oxides), the PE in this study delivered electric fields relying on the conductance of the plasma channels. The electric fields seem the best reason to cause the electroporation in the focal region. This was corroborated by three pieces of evidence. First, the electric field in the focal region was the highest and measured up to 1.5 kV/cm, although the actual field may be higher. The field is in the range of typical electroporation thresholds, 0.64 to 7 kV/cm, found in other studies.[13,25] Second, the effect of plasma chemistry, if dominating the electroporation, should occur elsewhere but the center, including the locations at the sites of the electrode projection.

As the plasma bombards the solution, the cell response at the anode and the cathode sides should be dominant. Instead, a focal electroporation at the center was observed. Third, the inability of the plasma channels to destroy the IC in the solution also suggests that the role of plasma chemistry is negligible compared with the pulse electric fields. However, the lack of decomposition of IC does not mean that there was no production of reactive oxygen and/or nitrogen species (RONS), neither does it prove an absence of biochemical effects. It may be that the RONS level required for IC decomposition was not reached or biochemical effects might occur at much lower levels. Moreover, some species may cause biochemical effects but not IC decomposition due to selective effects. As such, more follow-up studies are needed to clarify the roles of RONS.

The focused electroporation was mostly caused by the electric field formed by the positive and the negative plasma channels, being the maximum at the center below the electrodes, which is analogous to the field established by two elevated rod electrodes (Fig. 6a, b). The high field region, that is, the electrode tip, allowed the initiation of the plasma and did not make direct contact to the solution. The locations of the plasma contact with the solution may change randomly from pulse to pulse, unlike the fixed-positioned rods. Thus, the electrode footprints were eliminated, and a remote focused electroporation was created. We note that the electric field in Figure 6a and b is x-directed, which is the principal field that caused the electroporation. The vertical field (the z-component) did not play a major role, which would otherwise cause a strong electroporation directly under the electrodes. This observation suggests that the vertically directed field is harder to penetrate the solution than the horizontally directed field, presumably restricted by the surface charges.

The focused electroporation was only observed for a depth of 1.5 mm with the 300 ns plasma. Although increasing the pulse duration to 1 μs extended the electroporation to the increased depth (3 mm), the pattern no longer stayed focused. One reason is that the electric field decreases below the threshold value of electroporation, which depends on the combination of pulse numbers, electric field intensity, and pulse duration. As a result, a longer pulse duration means a lower electric field intensity required for electroporation. However, an arc/streamer plasma produced by 1 μs pulses can cause a much more complex electric field distribution than that by the 300 ns plasma. Therefore, a deeper level of focused electroporation may be possible with short pulses and higher voltages (such as 300 ns), provided that the plasma stays in the streamer mode. Because the field distribution in the interface between plasma and water is still an ongoing research subject, more research is needed to understand this complicated process.

There is a great body of literature that describes the use of plasma for biomedical applications. The plasma generation methods generally include dielectric barrier discharge, pulsed corona discharge, gliding arc discharge, plasma jet, and asymmetrical pulsed streamer discharges.[26] These plasma devices frequently involve inert gases, such as helium or argon, which favor the production of nonthermal plasma and electrochemically active species that are responsible for the bioeffects. Furthermore, these devices do not necessarily rely on the projected fields from the plasma, although recent research starts to accept the active role of the electric fields. In our experiments, the electric fields were the dominant mechanism for the membrane poration and the uptakes of Yo-pro-1 and PI.

The electric field measured in the large container (E_1) is expected to be different from that in the culture dish (E_2) as the two boundaries are different. Knowing the exact difference would take extensive efforts to model the plasma dynamics in each setting. However, with the measured currents, we can estimate that their magnitudes are quite close. The current density through the central plane between the electrode gap (i.e., the yz plane in the solution through which the current flows) is $J = \sigma E = I/S$, where I is the current, σ the conductivity of the solution, and S the area for current conduction. It can be shown that E_2/E_1 is I_2S_1/I_1S_2. Given $I_2 = 25$ A, $I_1 = 65$ A (peaks in Fig. 2), and the area S_1 being two to three times as S_2, as the field drops quickly from the depth of 1.5 to 3 mm, E_2/E_1 is estimated to be 0.76–1.15. In another less likely scenario when S_1 is much larger than S_2, E_2/E_1 becomes greater than 1.15, but they are still in the same order. Therefore, we can infer that the field inside the dish is close to the measured value in the container.

Finally, we comment on the shallower penetration of the electric field by the PE than by the ME. The electric field established by the ME is Coulomb's field, and the electrode polarization can be neglected due to the fact that nanosecond

pulses are much shorter than the electrode polarization time constant, which typically is in the range of >1 ms.[27] However, the field established by the PE, characterized by a much smaller interface relaxation time constant due to a smaller capacitance, is regulated by the electrical double layer between the plasma tip and the liquid.[28] Given a pulse longer than the charging time of the double layer, the electric field inside the liquid can be lost due to the dielectric screening.

This may be the case for the vertical fields as we have not measured significant Yo-pro-1 uptake directly on the electrode footprints (near the dashed line in Fig. 3). The impact of the double layer is that the field decreases exponentially [$E \propto \exp(-\kappa z)$, where κ^{-1} is the Debye length and is $<<1$ μm for a typical cell solution], faster than the inverse power of distance, typically found in the ME case. The faster decrease of the PE field is corroborated by the observation that the electroporation over depth caused by the PE decreased faster than the ME (Fig. 3).

Conclusions

The conventional method to deliver high-voltage pulses has been using solid electrodes, which results in a large electric field gradient throughout the gap, making the treatment nonuniform. Therefore, a focused regimen has been sought after to abate the inhomogeneity. We demonstrated *in vitro* that the delivery of nanosecond pulses through atmospheric pressure plasma channels allowed us to focus the electroporation on a culture dish away from the electrodes and therefore eliminating the electrode footprints. This concept was based on utilizing the leakage field projected from a pair of elevated electrodes emitting plasma streamers. We conclude that the duration of the electric pulse is critical to the focused electroporation.

In this case, the pulse duration of several hundreds of nanoseconds (e.g., 300 ns) was the best, when the plasma was in the streamer mode. Moreover, the cell depth for the focused electroporation is limited as found in this study to be 1.5 mm. The pulse duration of 1 μs allowed a broader and deeper electroporation at 3 mm, but the electroporation no longer stayed focused. Meanwhile, the physical mechanism for the focused electroporation is yet to be fully understood, although the electric field is considered as the primary mechanism. Using the PEs with varying pulse duration appears to be an interesting method of controlling the range of the electroporation, but the effectiveness on an *in vivo* target remains to be validated.

Acknowledgment

We thank Emily Gudvangen for taking some of the fluorescence images.

Authors' Contributions

S.X.: Designed, conducted the experiments, and wrote the article. C.Z.: Cultured cells, analyzed the data, and conducted the experiments. E.A.: Participated in the experiments. S.D.: Result interpretation.

Author Disclosure Statement

No competing financial interests exist.

Funding Information

This work was supported by the U.S. Air Force Office of Scientific Research (AFOSR) through an MURI project (FA9550-15-1-0517).

References

1. Weaver JC, Smith KC, Esser AT, et al. A brief overview of electroporation pulse strength-duration space: A region where additional intracellular effects are expected. Bioelectrochemistry 2012;87:236–243.
2. Yang E, Li J, Cho M, et al. Cell fragmentation and permeabilization by a 1ns pulse driven triple-point electrode. Biomed Res Int 2018;2018:4072983.
3. Roth CC, Barnes Jr RA, Ibey BL, et al. Characterization of pressure transients generated by nanosecond electrical pulse (nsEP) exposure. Sci Rep 2015;5(1):15063.
4. Klein N, Guenther E, Botea F, et al. The combination of electroporation and electrolysis (E2) employing different electrode arrays for ablation of large tissue volumes. PLoS One 2019;14(8):e0221393.
5. Appelbaum L, Ben-David E, Faroja M, et al. Irreversible electroporation ablation: Creation of large-volume ablation zones in in vivo porcine liver with four-electrode arrays. Radiology 2014;270(2):416–424.
6. Sano MB, DeWitt MR, Teeter SD, et al. Optimization of a single insertion electrode array for the creation of clinically relevant ablations using high-frequency irreversible electroporation. Comput Biol Med 2018;95:107–117.
7. Donate A, Coppola D, Cruz Y, et al. Evaluation of a novel non-penetrating electrode for use in DNA vaccination. PLoS One 2011;6(4):e19181.
8. Kos S, Vanvarenberg K, Dolinsek T, et al. Gene electrotransfer into skin using noninvasive multi-electrode array for vaccination and wound healing. Bioelectrochemistry 2017;114:33–41.
9. Gianulis EC, Casciola M, Zhou C, et al. Selective distant electrostimulation by synchronized bipolar nanosecond pulses. Sci Rep 2019;9(1):13116.
10. Pakhomov AG, Gudvangen E, Xiao S, et al. Interference targeting of bipolar nanosecond electric pulses for spatially focused electroporation, electrostimulation, and tissue ablation. Bioelectrochemistry 2021:107876.
11. Casciola M, Xiao S, Apollonio F, et al. Cancellation of nerve excitation by the reversal of nanosecond stimulus polarity and its relevance to the gating time of sodium channels. Cell Mol Life Sci 2019;76:4539–4550.
12. Valdez CM, Barnes Jr RA, Roth CC, et al. The interphase interval within a bipolar nanosecond electric pulse modulates bipolar cancellation. Bioelectromagnetics 2018;39(6):441–450.
13. Pakhomov AG, Grigoryev S, Semenov I, et al. The second phase of bipolar, nanosecond-range electric pulses determines the electroporation efficiency. Bioelectrochemistry 2018;122:123–133.
14. Valdez CM, Barnes Jr RA, Roth CC, et al. Asymmetrical bipolar nanosecond electric pulse widths modify bipolar cancellation. Sci Rep 2017;7(1):16372.
15. Pakhomov AG, Semenov I, Xiao S, et al. Cancellation of cellular responses to nanoelectroporation by reversing the stimulus polarity. Cell Mol Life Sci 2014;71(22):4431–4441.
16. Xiao S, Yamada R, Zhou C. Quadrupoles for remote electrostimulation incorporating bipolar cancellation. Bioelectricity 2020;2(4):382–390.

17. Xiao S, Semenov I, Petrella R, et al. A subnanosecond electric pulse exposure system for biological cells. Med Biol Eng Comput 2017;55(7):1063–1072.
18. Dhali SK. Generation of excited species in a streamer discharge. AIP Adv 2021;11(1):015247.
19. Guo B, Pomicter Anthony D, Li F, et al. Trident cold atmospheric plasma blocks three cancer survival pathways to overcome therapy resistance. Proc Natl Acad Sci U S A 2021;118(51):e2107220118.
20. Athos BG, Uecker DR, Xiao S. High-voltage analog circuit pulser and pulse generator discharge circuit. US Patent 2020;10874451.
21. Xiao S, Athos BG, Kreis MP, et al. High-voltage analog circuit pulser with feedback control. US Patent 2020; 10548665.
22. Pakhomov AG, Bowman AM, Ibey BL, et al. Lipid nanopores can form a stable, ion channel-like conduction pathway in cell membrane. Biochem Biophys Res Commun 2009;385(2):181–186.
23. Ruma, Hosano H, Sakugawa T, et al. The role of pulse voltage amplitude on chemical processes induced by streamer discharge at water surface. Catalysts 2018;8(5):213.
24. Crema APS, Piazza Borges LD, Micke GA, et al. Degradation of indigo carmine in water induced by non-thermal plasma, ozone and hydrogen peroxide: A comparative study and by-product identification. Chemosphere 2020;244:125502.
25. Pakhomov AG, Xiao S, Novickij V, et al. Excitation and electroporation by MHz bursts of nanosecond stimuli. Biochem Biophys Res Commun 2019;518(4):759–764.
26. Perinban S, Orsat V, Raghavan V. Nonthermal plasma–liquid interactions in food processing: A review. Compr Rev Food Sci Food Saf 2019;18(6):1985–2008.
27. González A, Ramos A, Green NG, et al. Fluid flow induced by nonuniform ac electric fields in electrolytes on microelectrodes. II. A linear double-layer analysis. Phys Rev E 2000;61(4):4019–4028.
28. Vanraes P, Bogaerts A. The essential role of the plasma sheath in plasma–liquid interaction and its applications—A perspective. J Appl Phys 2021;129(22):220901.

Address correspondence to:
Shu Xiao, PhD
Frank Reidy Research Center for Bioelectrics
Old Dominion University
Norfolk, VA 23508
USA

E-mail: sxiao@odu.edu